NUMERICAL PREDICTION OF AIR FLOW IN A SHARP 90º ELBOW.

Ruth MOSSAD[1], William YANG[2], M. Philip SCHWARZ[2]

[1] University of Southern Queensland, Toowoomba, QLD 4350, AUSTRALIA

[2]CSIRO Process Science and Engineering, Clayton, Victoria 3168, AUSTRALIA

ABSTRACT

Numerical and experimental investigations of turbulent air flows inside a sharp 90° elbow bend were conducted in an open-circuit horizontal-to-vertical suction wind tunnel system. Computational fluid dynamics simulations were performed using Fluent software with 3D, steady, turbulent and incompressible flow conditions assumed. Three different turbulence models were used namely the k-ε realizable, the *k*-ε RNG and the Reynolds Stress models in conjunction with non-equilibrium wall functions. The predictions of mean velocity profiles of the air flow inside the sharp 90° elbow duct were compared against the experimental results obtained using Laser Doppler Anemometry (LDA). Reasonable agreement was obtained. Reynolds Stress Model was expected to perform the best; however this was not confirmed from the results.

NOMENCLATURE

a characteristic length
g   acceleration of gravity
p pressure
U_x horizontal mean velocity of air flow
U_z vertical mean velocity of air flow
$\vec{v}$ velocity vector
ρ density
μ dynamic viscosity
τ Stress tensor

INTRODUCTION

It is common that the air-conditioning and ventilation duct systems and the mill-duct conveying systems consist of not only curved 90° elbow bends with various curvature ratios, but also right-angled sharp 90° elbow bends due to space limitations. Curved elbows cause less energy losses than sharp elbows; however their production is more costly. Energy losses in sharp elbows are caused by the formation of a separation zone, which appears just after the corner. The stability of this separation zone is questionable, which makes the numerical prediction of the flow in sharp elbows difficult.

Owing to the complexity of the flow structure inside the elbows, coupled with the limitations of experimental measurement and CFD techniques, a complete understanding of the turbulent air flow behaviour in such systems is lacking. This is particularly the case with the right-angled sharp 90° elbow bends. However, there are a number of detailed experimental and numerical studies related to the single phase air flow and gas-particulate two-phase flows with curved 90° elbow bends. Humphrey

et al. (1981) reported the first comprehensive air flow velocity measurements using LDA for a square-sectioned curved 90° elbow bend. It was found that the secondary motion causes strong cross-stream convection of Reynolds stresses, and drives the fluid flow that contains higher turbulence energy from the outer wall where flow is destabilised by the concave curvature towards the inner wall. The mean flow is however strongly influenced by the pressure forces and hence the use of standard eddy-viscosity models, which are unable to resolve negative contributions to the generation of turbulence kinetic energy, are expected to become inadequate for predicting strongly curved flows.

As an extension to the study of Humphrey *et al.*, Taylor *et al.* (1982) examined the influence of developing entry flow under laminar and turbulent regimes. In addition, the authors also compared the development of secondary flow in square-sectioned elbows with varying degree of curvature. From the experiment, they established that the core flow develops under the separate influences of the streamwise pressure gradients and cross-stream convection by the secondary flow.

Yilmaz and Levy (2001) carried out a detailed numerical and experimental investigation in the formation and dispersion of roping following a curved 90° elbow in a pneumatic conveying system. They have identified a number of parameters that affect rope flow formation and dispersion in the vertical pipe following a horizontal-to-vertical elbow. These include elbow radius, air flow velocity, solid mass loading as well as the pipe diameter. With the aid of a commercial CFD package CFX-FLOW3D, Yilmaz and Levy illustrated the importance of particle-wall collisions in the prediction of flows through a curved elbow. They also demonstrated the secondary flow pattern with the use of CFD and explain the importance of individual effect of secondary flows as well as local turbulence in dispersing the rope flow.

Recently, Yang & Kuan (2006) and Kuan *et al.* (2006) carried out experimental and numerical investigations of dilute turbulent particulate flows inside a curved 90° elbow bend. The particulate flow was found to behave differently from the air flow near the outer wall of the curved duct due to the presence of particle-wall collisions which contributed to a strong transverse particle velocity away from the outer wall downstream of the bend. The numerical turbulent gas flow solution based on differential Reynolds stress modelling (DRSM) provided a reasonable representation of the mean air flow comparing to the

experimental data, except in regions next to the concave wall of the bend.

As an extension to Yang and Kuan's study, this paper summarises the numerical and experimental investigations of turbulent air flows inside a right-angled sharp 90° elbow bend. The CFD predictions of mean velocity profiles of the air flow inside the sharp 90° elbow bend were compared against the experimental results obtained using Laser Doppler Anemometry (LDA).

EXPERIMENTAL APPARATUS

All LDA experimental measurements inside the right-angled sharp 90° elbow were conducted in an open-circuit horizontal-to-vertical suction wind tunnel system located at CSIRO Process Science and Engineering. Detailed description of the set-up was given by Yang and Kuan (2006). The 150×150 (mm^2) square test section was constructed using 10mm thick Perspex, and consisted of a 3.5m-long horizontal straight duct, a right-angled sharp 90° elbow, and a 1.8m-long vertical straight duct. The geometry of the test section, the sharp 90° elbow, and the locations of LDA measurements taken are shown in Figure 1.
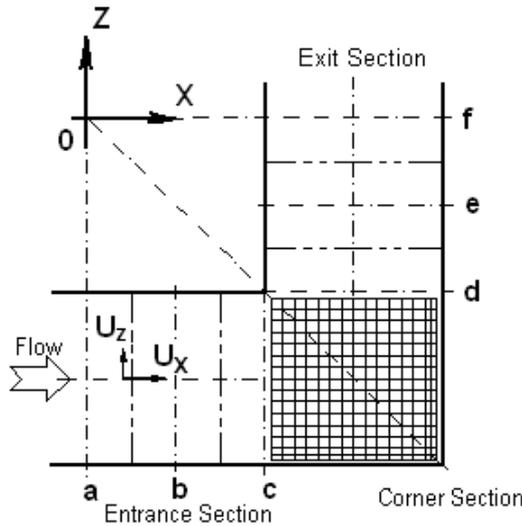

Figure 1: Schematic diagram of sharp 90° elbow section

Experimental results presented in this paper were for a bulk gas velocity of 10m/s in the duct system which corresponds to a Reynolds number about 10^5. The turbulence intensity in the main stream was about 1% at the centre of the duct cross-section 10D upstream of the 90° bend. As the seeding particles for the gas phase, a fine mist of sugar particles with a mean diameter about 1 μm were generated by a TSI six-jet Atomizer from a 5% sugar solution. It was found that the seeding particles tracked the gas flow well with an aerodynamic response time of approximately 10 μs. This is in accordance with the smallest time scale for gas flow fluctuations in the flow.
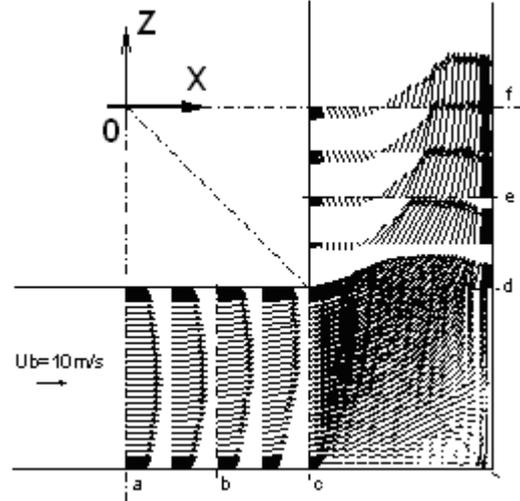

Figure 2: Velocity vectors of gas-phase inside a right-angled sharp 90° elbow

The TSI-Aerometrics 2D back-scattering LDA system was employed for the experimental measurements. The LDA system consists of a two-colour four-beam optical arrangement utilising the green (wave length = 514.5 nm) and blue (wave length = 488 nm) lines of a 5W Argon-Ion laser. The fibre optics had a lens of a 250 mm focal length and a 40 mm beam separation which produced an ellipsoid shaped measurement volume. The system is capable of simultaneously determining the time mean horizontal and vertical velocities U_x and U_z, and the RMS of their fluctuating components. Figure 2 illustrates the vectors of gas-phase mean horizontal and vertical velocities obtained from LDA measurements inside the right-angled sharp 90° elbow. The total estimated uncertainties using the current LDA system were 3% for the mean velocities and 7% for the fluctuating components respectively.

MATHEMATICAL MODEL

The governing equations namely conservation of mass and momentum, in differential form for incompressible, steady, isothermal, three-dimensional, turbulent flow are given below:

$$\nabla.\left(\rho\vec{v}\right) = 0 \qquad (1)$$

$$\nabla.\left(\rho\vec{v}\vec{v}\right) = \rho\vec{g} - \nabla p + \nabla.\left(\bar{\bar{\tau}}\right) + \nabla.\left(-\rho\overline{\vec{v}'\vec{v}'}\right) \quad (2)$$

In these equations, $\vec{v}$ is the average velocity vector which has the components u, v and w in the x, y and z directions, p is the average static pressure, ρ and g are the density and the acceleration of gravity. Equation (2) is the time-averaged Navier-Stokes equation for turbulent flow in which $\nabla.\left(-\rho\,\overline{v'v'}\right)$ is the Reynolds stresses, which depends on the turbulence model chosen, and $\bar{\bar{\tau}}$ is the stress tensor given as follows:

$$\bar{\bar{\tau}} = \mu\left[\left(\nabla\vec{v} + \nabla\vec{v}^T\right) - \frac{2}{3}\nabla.\vec{v}I\right] \qquad (3)$$

where μ is the fluid viscosity, and I is the identity matrix.

2

The governing equations are non-linear partial differential equations for which a closed form solution is not possible. The computational fluid dynamics software "Fluent", which uses a control volume-based finite difference method, was chosen to solve these equations, due to its general capability, user-friendliness, and availability to the author.

Three turbulent models were used in this work to examine which one predicts the flow most closely to the values measured at the advanced Laser Diagnostic Laboratory at CSIRO. These turbulent models are the k-ε realizable (Shih *et al*, 1995), the k-ε RNG (Yakhot & Orszag, 1986 and Choudhury, 1993), and the Reynolds stress model (Speziale *et al*, 1991).

The k-ε model is a semi-empirical model based on model transport equations for turbulent kinetic energy k and its dissipation rate ε. In Fluent there are the standard, the realizable and the RNG k-ε models. The last two are improved version of the standard k-ε model which suits fully turbulent flow problems. In regard to the k-ε realizable, the term "realizable" means that the model satisfies certain mathematical constraints on the Reynolds stresses, consistent with the physics of turbulent flows, (Shih *et al*, 1995). This turbulence model provides superior performance for flows involving rotation, boundary layers under strong adverse pressure gradients, separation, and recirculation.

The k-ε RNG model is derived using a statistical technique called the renormalization group theory; details and its application can be found in Choudhury (1993). It provides improved results compared with the standard k-ε in the case of streamline curvature, rapidly strained and swirling flow. It also allows for low-Reynolds-number effects. Effective use of this feature does, however, depend on an appropriate treatment of the near-wall region.

The Reynolds Stress Model (RSM) is the most elaborate turbulence model. The RSM closes the Reynolds-averaged Navier-Stokes equations by solving transport equations for the Reynolds stresses, together with an equation for the dissipation rate. This means that seven additional transport equations must be solved in 3D problems. The Reynolds stress model was chosen with the quadratic pressure-strain relationship proposed by Speziale *et al.* (1991), which treats flow with streamline curvature, swirl, rotation, and rapid changes in strain rate in a more rigorous manner than one-equation and two-equation models (e.g. the k-ε models); i.e. it is expected to give accurate predictions for complex flows.

The non-equilibrium wall function was chosen with all turbulent models which uses a two-layer approach to include the pressure-gradient effects. The wall-neighbouring cells are assumed to consist of a viscous sublayer and a fully turbulent layer. The two-layer approach is chosen to compute the turbulence kinetic energy budget in the wall-neighbouring cells using Lauder and Spalding's log-law for mean velocity that is sensitized to pressure gradient effect; details can be found in (Kim & Choudhury, 1995). The first order upwind discretization was chosen for the momentum, turbulent kinetic energy and turbulence dissipation rate while the PRESTO discretization (PREssure STaggering Option) was chosen for the pressure since it is more appropriate for flow with swirl (according to Patankar, 1980) and the SIMPLE method (Semi-Implicit Method for Pressure-Linked Equations) algorithm, was chosen for the pressure velocity coupling.

Boundary conditions used at the inlet were a fully developed velocity profile (which was obtained by solving a flow in a square long duct with 0.15 m side with uniform velocity at inlet: a velocity distribution at a depth of around 11D from the inlet was chosen to represent fully developed flow). The exit was considered as an outlet, meaning that the flow would come out of the duct with velocity parallel to the walls of the duct. On the walls the non-slip condition was assumed with an average wall roughness height of 4.6×10^{-5} m.

RESULTS

A 3-D ducting system model consisting of a sharp 90° elbow of 150×150 (mm^2) square cross section, a 3.5 m horizontal section and 1.9m vertical section similar to the experimental setup was generated using Gambit software. A variable size hexahedral mesh was generated, with a finer mesh generated in the corner to allow more accurate prediction in the region of large variation of velocities and pressures due to the large turning angle of the flow around the corner, and also close to the wall boundaries to accurately predict the boundary layer close to the walls.

Different size meshes were generated in the range 500,000 -5,000,000: this was to obtain results that are independent of the mesh size. Velocities in the vertical direction (z direction) at four different locations in the sharp elbow, d, e, and f and at 3D downstream, were obtained using the realizable turbulent model for the different size mesh to study the convergence of the solution as the mesh gets finer. A convergence criterion for all parameters was taken as 10^{-4}. These were also compared to the experimental results obtained using LDA at CSIRO. The results are presented in Figures 3-6.
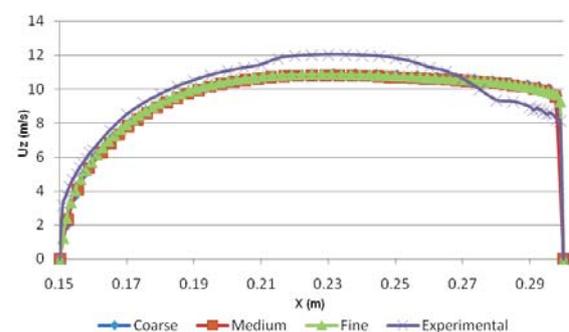

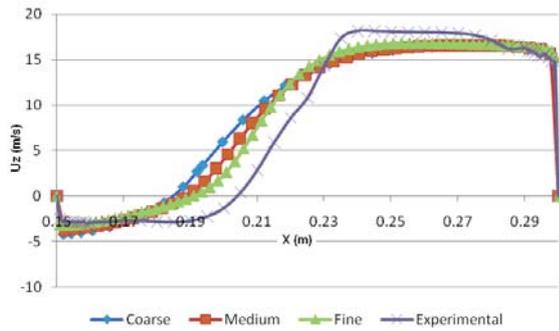**Figure 3:** Effect of mesh size on CFD prediction of vertical velocities in d-section.

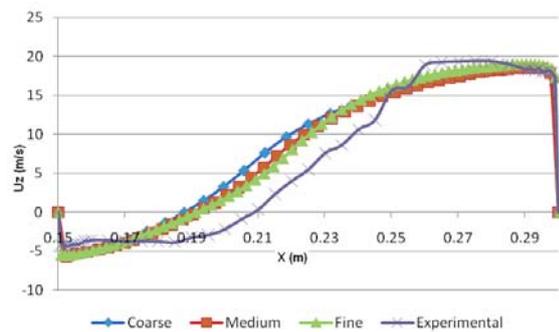**Figure 4:** Effect of mesh size on CFD prediction of vertical velocities in e-section.

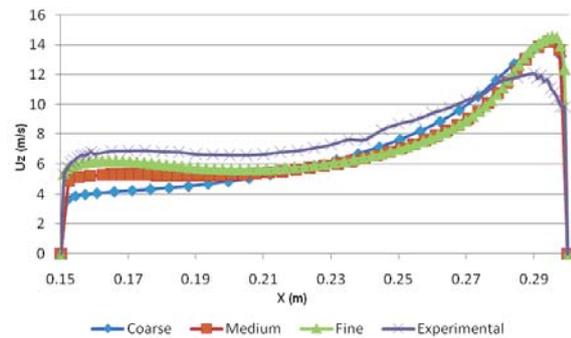**Figure 5:** Effect of mesh size on CFD prediction of vertical velocities in f-section.

Figure 6: Effect of mesh size on CFD prediction of vertical velocities at 3D downstream section.

Comparing with the experimental results, one can see that in section d the improvement in the velocity values using a finer mesh were very little, while in the sections e and f the improvements were more obvious in the middle of the duct, while in section 3D (which is three duct widths from the exit of the corner) the improvement was more pronounced in the zone close to the inside wall of the duct.

Velocities in the vertical direction (z direction) at the same four locations in the sharp elbow were obtained using the different turbulent models and compared to the experimental results obtained at CSIRO Clayton laboratories. The results for the case with 4,899,300 nodes for which there are 73x73 nodes in the cross section, are shown in Figures 7-10. Convergence criteria for all parameters were taken as 10^{-4} for the realizable k-ε model and the Reynolds stress turbulent model, however for the

k-ε RNG turbulent model a converged solution at 10^{-3} was obtained, however lower convergence levels could not be reached, even when varying relaxation factors.

Comparing the above velocity profiles, one can observe that none of the turbulent models perfectly matched the experimental data; however for section d the three models behaved very close to each other, while the Reynolds stress model compared more favourably than the realizable and RNG in sections e and f. In section 3D, however, the realizable k-ε model gave the best results.
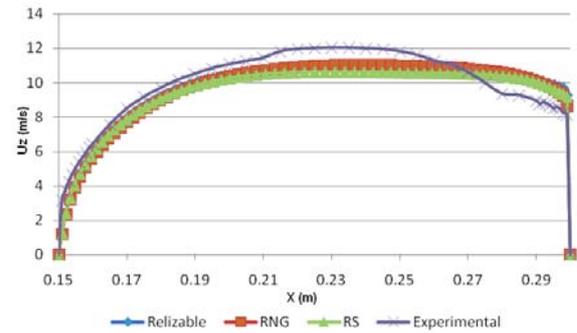

Figure 7: Comparisons for Z velocity at middle line in d-section using three turbulence models
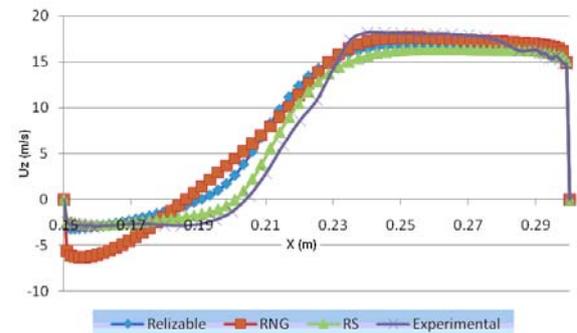

Figure 8: Comparisons for Z velocity at middle line in e-section using three turbulence models
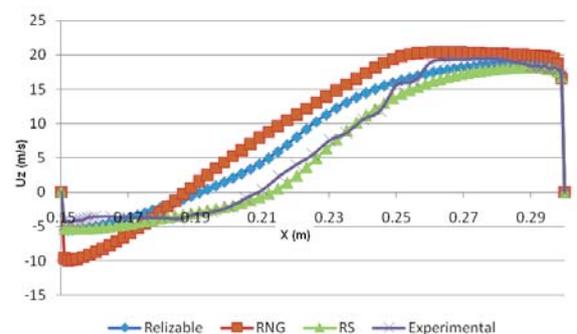

Figure 9: Comparisons for Z velocity at middle line in f-section using three turbulence models
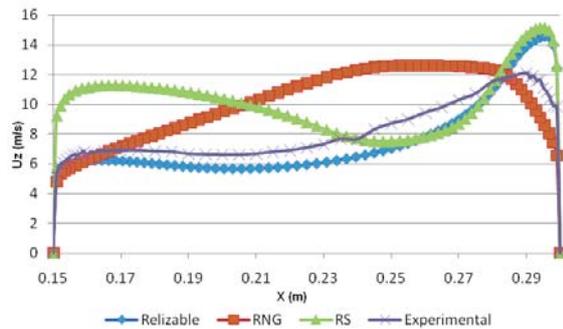
Figure 10: Comparisons for Z velocity at middle line at 3D downstream section using three turbulence models

Velocity vectors at the mid-plane of the sharp elbow are shown in Figure 11. The velocity vectors show the separation zone in the flow which starts right after the sharp corner of the elbow.
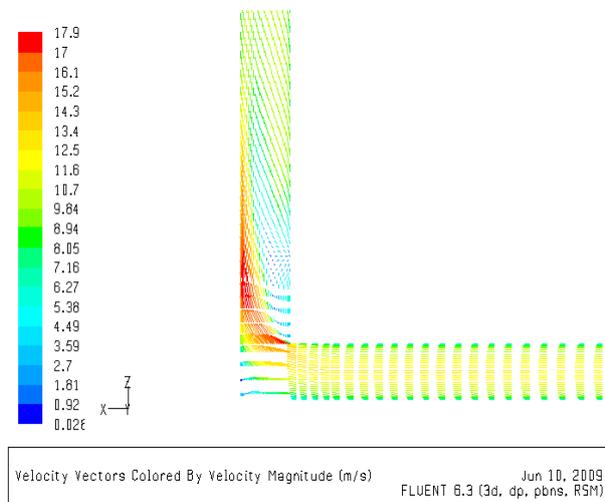

Figure 10: Velocity vectors at middle plane using coarse mesh with RSM

CONCLUSIONS

The behaviour of mean turbulent air flows inside a right-angled sharp 90° elbow bend system have been studied using LDA as well as numerical simulation. Experimental data has been successfully applied to validate the numerical predictions based on three different turbulence models, the k-ε realizable, the k-ε RNG and the Reynolds Stress models in conjunction with non-equilibrium wall functions. Reasonable agreement was obtained. The Reynolds Stress Model was expected to perform the best; however this was not confirmed from the results. While the Reynolds Stress Model gave the best prediction for the region immediately downstream of the elbow including the flow separation and recirculation, the k-ε realizable model performed better further downstream, as the flow profile recovered towards developed flow. The comparison between the calculated and experimental data indicates a need to further modify the turbulence model if better flow prediction is to be achieved in the future.

REFERENCES

CHOUDHURY, D., (1993), "Introduction to the renormalization group method and turbulence modelling", *Fluent Inc. Technical Memorandum,* TM-107.

KIM, S.-E. and CHOUDHURY, D., (1995), "A near-wall treatment using wall functions sensitized to pressure gradient", *ASME FED, Separated and Complex Flows,* **217**.

HUMPHERY, J.A.C., WHITELAW, J.H. and YEE, G., (1981), "Turbulent flow in a square duct of strong curvature", *J. Fluid Mechanics*, **103**, 443–463.

KUAN, B., YANG, W. and SCHWARZ, M.P., (2007), "Dilute gas-solid two-phase flows in a curved 90° duct bend: CFD simulation with experimental validation", *Chemical Engineering Science*, **62**, 2068–2088.

PATANKAR, S.V., (1980), "Numerical Heat Transfer and Fluid Flow", Hemisphere, Washington DC.

SHIH, T.–H., LIOU, W.W. SHABBIR, A., YANG, Z. and ZHU, J., (1995), "A new k-ε eddy-viscosity model for high Reynolds number turbulent flows - Model development and validation", *Computers Fluids*, **24(3)**, 227–238.

SPEZIALE, C.G., SARKAR, S. and GATSKI, T.B., (1991), "Modelling the pressure-strain correlation of turbulence: An invariant dynamical systems approach", *J. Fluid Mech.*, **227**, 245–272.

TAYLOR, A.M.K.P., WHITELAW, J.H. and YIANNESKIS, M., (1982), "Curved ducts with strong secondary motion: velocity measurements of developing laminar and turbulent flow", *J. Fluids Engineering*, **104**, 350–359.

YAKHOT, V. and ORSZAG, S.A., (1986), "Renormalization group analysis of turbulence: I. Basic theory", *J. Scientific Computing*, **1(1)**, 1–51.

YANG, W. and KUAN, B., (2006), "Experimental investigation of dilute turbulent particulate flow inside a curved 90° bend", *Chemical Engineering Science*, **61**, 3593–3601.

YILMAZ, A. and LEVY, E. K., (2001), "Formation and dispersion of ropes in pneumatic conveying", *Powder Technology*, **114**, 165–185.